Journal of Hydrology 452–453 (2012) 213–225

Contents lists available at SciVerse ScienceDirect

Journal of Hydrology

journal homepage: www.elsevier.com/locate/jhydrol

Comprehensive evaluation of multi-satellite precipitation products with a dense rain gauge network and optimally merging their simulated hydrological flows using the Bayesian model averaging method

Shanhu Jiang [a], Liliang Ren [a,*], Yang Hong [b], Bin Yong [a], Xiaoli Yang [a], Fei Yuan [a], Mingwei Ma [a]

[a] State Key Laboratory of Hydrology – Water Resources and Hydraulic Engineering, Hohai University, Nanjing 210098, China
[b] School of Civil Engineering and Environmental Sciences and School of Meteorology, University of Oklahoma, Norman, OK, USA

ARTICLE INFO

Article history:
Received 27 September 2011
Received in revised form 31 March 2012
Accepted 26 May 2012
Available online 4 June 2012
This manuscript was handled by Konstantine P. Georgakakos, Editor-in-Chief, with the assistance of Ashish Sharma, Associate Editor

Keywords:
Satellite precipitation
Hydrological modeling
Streamflow
Bayesian model averaging

SUMMARY

This study first focuses on comprehensive evaluating three widely used satellite precipitation products (TMPA 3B42V6, TMPA 3B42RT, and CMORPH) with a dense rain gauge network in the Mishui basin (9972 km^2) in South China and then optimally merge their simulated hydrologic flows with the semi-distributed Xinanjiang model using the Bayesian model averaging method. The initial satellite precipitation data comparisons show that the reanalyzed 3B42V6, with a bias of −4.54%, matched best with the rain gauge observations, while the two near real-time satellite datasets (3B42RT and CMORPH) largely underestimated precipitation by 42.72% and 40.81% respectively. With the model parameters first benchmarked by the rain gauge data, the behavior of the streamflow simulation from the 3B42V6 was also the most optimal amongst the three products, while the two near real-time satellite datasets produced deteriorated biases and Nash–Sutcliffe coefficients (NSCEs). Still, when the model parameters were recalibrated by each individual satellite data, the performance of the streamflow simulations from the two near real-time satellite products were significantly improved, thus demonstrating the need for specific calibrations of the hydrological models for the near real-time satellite inputs. Moreover, when optimally merged with respect to the streamflows forced by the two near real-time satellite precipitation products and all the three satellite precipitation products using the Bayesian model averaging method, the resulted streamflow series further improved and became more robust. In summary, the three current state-of-the-art satellite precipitation products have demonstrated potential in hydrological research and applications. The benchmarking, recalibration, and optimal merging schemes for streamflow simulation at a basin scale described in the present work will hopefully be a reference for future utilizations of satellite precipitation products in global and regional hydrological applications.

1. Introduction

Precipitation is arguably the vital input data for various hydrologic models. Obtaining accurate and reliable precipitation data is thus very important for local, regional and global hydrologic prediction and water resources management. Traditionally, the acquisition of precipitation data is often limited to ground-based observations (using rain gauges and/or ground-based weather radars) although these surface-based observations usually suffer from low spatial coverage, especially in developing regions where ground-based observations are rare or even unavailable. For the past dozen years, a great deal of effort has been devoted to the development of space-based new observation platforms and retrieval methods for estimating accurate and globally available precipitation products at relatively high spatial and temporal resolutions.

Recently, a number of new global high resolution satellite-based precipitation products have been operationally available, including the Precipitation Estimation from Remotely Sensed Information using Artificial Neural Networks (PERSIANN; Sorooshian et al., 2000), the National Oceanic and Atmospheric Administration Climate Prediction Center morphing technique product (CMORPH; Joyce et al., 2004), the PERSIANN-Cloud Classification System estimation (PERSIANN-CCS; Hong et al., 2004), the Naval Research Laboratory Global Blended-Statistical Precipitation Analysis data (NRL-Blend; Turk and Miller, 2005), the Global Satellite Mapping of Precipitation (GSMaP; Kubota et al., 2007), the Tropical Rainfall Measuring Mission (TRMM) Multi-satellite Precipitation Analysis products (TMPA; Huffman et al., 2007), and so on. These satellite precipitation products have provided quasi-global high-temporal (⩽3 h) and spatial (⩽0.25°) resolution

* Corresponding author. Tel.: +86 25 83787480.
E-mail address: njrll9999@126.com (L. Ren).

0022-1694/$ - see front matter © 2012 Elsevier B.V. All rights reserved.
http://dx.doi.org/10.1016/j.jhydrol.2012.05.055

precipitation maps. The PERSIANN has been generated from March 2000 to present; the CMORPH has been produced from December 2002 to present; the PERSIANN_CCS has been utilized from 2005 to present; the NRL-Blend has been generated from mid-2000 to present; the GSMaP has been used since 2005; and the TMPA 3B42RT and 3B42V6 have been available since January 2002 and January 1998, respectively. As anticipated, the expended follow-on project of the TRMM, the Global Precipitation Measurement (GPM; http://pmm.nasa.gov/GPM) mission will provide more coverage and more accurate precipitation product so as to further improve our capacity of retrieving precipitation from space.

Nevertheless, satellite precipitation products need be evaluated against in situ observations and then calibrated to various hydrological models before full-scale deployment and application to daily and sub-daily hydrological operations. Direct comparisons of various satellite precipitation products with a dense rain gauge network and/or ground radar observations have been conducted (Tian et al., 2007; Chokngamwong and Chiu, 2008; Dinku et al., 2008; Yu et al., 2009; Jiang et al., 2010). On the other hand, numerous studies have evaluated various satellite precipitation products for streamflow simulation (Hong et al., 2007; Su et al., 2008; Stisen and Sandholt, 2010; Yong et al., 2010, 2012; Behrangi et al., 2011). There also have been some inter-comparison projects which aimed to evaluate the performance of the satellite precipitation products. Amongst, the most typical one is the Program of Evaluation of High-Resolution Precipitation Products (PEHRPP; Turk et al., 2008) established by the International Precipitation Working Group (IPWG). These studies and projects emphasized that satellite precipitation products have certain accuracy and great potential for hydrologic applications. It is important to note, however, that different types of satellite precipitation data might have variable accuracy and thus distinct hydrological utility in different regions. This plays a role in determining which precipitation product is most optimal for certain regions. The task at hand though proved to be difficult because of the inconsistency among satellite observations and retrieval algorithms as well. How to identify these optimal satellite products and how to achieve the best possible streamflow simulation forced by a suite of satellite precipitation products has been a challenge.

There have been some attempts that tried to improve the streamflow simulation by merging multiple precipitation products. Chiang et al. (2007) combined the gauge observations and satellite precipitation products by a recurrent neural network (RNN) method to enhance the accuracy of the flood forecasting. Li and Shao (2010) used a nonparametric kernel smoothing method to merge satellite rainfall estimates and rain gauge observations to improve the accuracy of the regional rainfall estimation. Yilmaz et al. (2010) merged the multi-precipitation products by minimizing the simulated land surface parameter (soil moisture, temperature, etc.) errors with the downhill simplex method to improve the land surface simulation. Gebregiorgis and Hossain (2011) used a priori hydrological model predictability method to merge three near real-time satellite precipitation products to improve the hydrologic prediction. These methods are conducted from merging the different satellite precipitation products or with the gauge observations. However, when the satellite precipitation products existing large deviations and/or there are no rain gauge observations, these methods may be noneffective. The hydrological model can tolerate the errors of the satellite precipitation products through its nonlinear system by adjusting the model parameters (Stisen and Sandholt, 2010; Bitew and Gebremichael, 2011). So merging the simulations from multi-satellite precipitation products is a novel method to improve the streamflow simulations or predictions, especially for the data-spare and ungauged basins.

The current study thus focused on two aspects. First, three most widely used global high-resolution satellite precipitation products (TMPA 3B42V6, TMPA 3B42RT, and CMORPH, 3 h and 0.25°) were compared in detail with the dense rain gauge network observations and their streamflow simulation utilities were comprehensively evaluated using the semi-distributed Xinanjiang mode during the period of 2003–2008 in the Mishui basin (9972 km^2) in South China. Second, the simulated streamflows from the different satellite precipitation products were optimally merged using the Bayesian model averaging method (BMA; Ajami et al., 2007; Duan et al., 2007), through which the advantages of the simulations from different satellite precipitation products were capitalized. The present work is organized as follows: Section 2 describes the detailed methodology; Section 3 introduces the study area and the data sets used; Section 4 presents the results and discussion; and Section 5 draws the conclusions.

2. Methodology

2.1. Evaluation statistics

To qualitatively evaluate the three satellite precipitation products with dense surface rain gauge observations, five widely used validation statistical indices were adopted in the present study. The mean error (ME) was used to scale the average difference between the satellite precipitation and rain gauge observations, whereas the mean absolute error (MAE) was used to represent the average magnitude of the error. The relative bias (BIAS) describes the systematic bias of the satellite precipitation. The correlation coefficient (CC) was used to assess the agreement between the satellite precipitation and rain gauge observations. The root mean square error (RMSE), which gives a greater weight to the larger errors relative to MAE, was used to measure the average error magnitude. The formulas are given by:

$$ME = \frac{1}{n}\sum_{i=1}^{n}(S_i - G_i) \tag{1}$$

$$MAE = \frac{1}{n}\sum_{i=1}^{n}|(S_i - G_i)| \tag{2}$$

$$BIAS = \frac{\sum_{i=1}^{n}(S_i - G_i)}{\sum_{i=1}^{n}G_i} \times 100\% \tag{3}$$

$$CC = \frac{\sum_{i=1}^{n}(G_i - \overline{G})(S_i - \overline{S})}{\sqrt{\sum_{i=1}^{n}(G_i - \overline{G})^2}\sqrt{\sum_{i=1}^{n}(S_i - \overline{S})^2}} \tag{4}$$

$$RMSE = \sqrt{\frac{1}{n}\sum_{i=1}^{n}(S_i - G_i)^2} \tag{5}$$

where n is the total amount of rain gauge or satellite precipitation data; S_i and G_i are the ith values of the satellite precipitation data and rain gauge observations, respectively; and $\overline{S}$ and $\overline{G}$ are the mean values of the satellite precipitation data and rain gauge observations, respectively.

In addition, three categorical statistical indices, including the probability of detection (POD), false-alarm rate (FAR), and critical success index (CSI) were adopted to measure the correspondence between the satellite precipitation products and rain gauge observations. POD, also known as the hit rate, represents how often the rain occurrences are correctly detected by the satellite. FAR denotes the fraction of cases in which the satellite records precipitation when the rain gauges do not. CSI shows the overall fraction of precipitation events correctly diagnosed by the satellite.

Rain or no-rain events were defined by the value of the threshold, and a precipitation threshold of 1.0 mm was used in this study. The perfect values of POD, FAR and CSI were 1, 0, and 1, respectively. The formulas are given by:

$$POD = \frac{t_H}{t_H + t_M} \tag{6}$$

$$FAR = \frac{t_F}{t_H + t_F} \tag{7}$$

$$CSI = \frac{t_H}{t_H + t_M + t_F} \tag{8}$$

where H, M, and F are different cases: H, observed rain correctly detected; M, observed rain not detected; F, rain detected but not observed; and t_H, t_M and t_F are the times of occurrence of the corresponding case; the details of these are referred to Ebert et al. (2007).

The validation statistical indices of CC, BIAS and the Nash–Sutcliffe coefficient (NSCE; Nash and Sutcliffe, 1970) were employed to evaluate the hydrologic model performance based on the observed and simulated streamflow series. CC, BIAS and NSCE jointly measure the consistency of the simulated and observed streamflow series both in terms of the temporal distribution and amount. The formula for NSCE is given by:

$$NSCE = 1 - \frac{\sum_{i=1}^{n}(Q_{sim}(i) - Q_{obs}(i))^2}{\sum_{i=1}^{n}(Q_{obs}(i) - \bar{Q}_{obs})^2} \tag{9}$$

where $Q_{obs}(i)$ is the observed runoff at time step i, $Q_{sim}(i)$ is the simulated runoff at time step i, $\bar{Q}_{obs}$ is the mean value of the observed values, and n is the number of data points.

2.2. Hydrological model and calibration

The Xinanjiang model is a well known physically based conceptual hydrological model (Zhao, 1992) that has been successfully and widely used in the humid and semi-humid regions of China since its development in the 1970s. Recently, the runoff generation method of this model has been widely used in distributed hydrological simulations. The core of the model, which describes their spatial heterogeneity of tension water and free water within a basin based on the storage capacity distribution curves, was employed by the three-layer Variable Infiltration Capacity (VIC-3L) model (Liang et al., 1994, 1996).

In the present work, a gridded-structured Xinanjiang model for streamflow simulation was constructed. The simulation was performed by computing the runoff and dividing the runoff types within each grid. The slope and river network convergence processes were then integrated to obtain the streamflow series of the hydrologic station. The gridded Xinanjiang model was operated daily with a $0.25^\circ \times 0.25^\circ$ spatial resolution from January 2003 to December 2008. The Xinanjiang model has 16 parameters and their physical meanings, numeric ranges and default values are shown in Table 1.

The model parameters were automatically calibrated using the Shuffled Complex Evolution Metropolis (SCEM-UA, Vrugt et al., 2003). The SCEM-UA was built upon the principles of the Shuffled Complex Evolution (SCE-UA), an effective and efficient global optimization technique developed by Duan et al. (1994). The SCEM-UA combined the strengths of the Monte Carlo Markov Chain sampler with the concept of complex shuffling from SCE-UA to form an algorithm that not only provides the most probable parameter set, but also estimates the uncertainty associated with estimated parameters. The SCEM-UA was able to simultaneously identify the most likely parameter set and its associated posterior probability distribution in every model run (Ajami et al., 2007). In this study, the initial samples and the compute times were set at 5000 and 10,000, respectively.

2.3. Simulation scenarios

Model calibration is a process that optimizes parameters to obtain the best simulation of observed natural runoff for certain forcing data. Different forcing data have different temporal and spatial biases compared with the unknown true values. The model parameters may present some variations when used to simulate the streamflow (Stisen and Sandholt, 2010). Different forcing data could result in similar streamflow simulations after calibration based on each input data. In the current study, two simulation scenarios were thus set to evaluate the streamflow simulation utility of the three satellite precipitation products. In Scenario I, the Xinanjiang model parameters were calibrated with the rain gauge precipitation measurements and the model runs were repeated with the three satellite precipitation products as inputs. In Scenario II, these parameters were recalibrated with each of the satellite precipitation products. The simulations from Scenario II were then merged using the BMA method.

2.4. Merging method

The BMA is a probabilistic scheme for model combinations that derives the consensus prediction from competing predictions using likelihood measures as model weights (Ajami et al., 2007). The BMA weights are directly bound with the individual model simulation. A more robust and stable result can be obtained when the BMA method is used to combine the different simulations. Each satellite precipitation product has its own merit in terms of capturing real rainfall events. With different satellite precipitation products as input forcing data, the hydrological model can generate various streamflow series with different accuracy. Merging the different satellite data forced streamflow simulations using the BMA method is hence considered a novel method that may generate a better, more stable streamflow series.

3. Study area and data

3.1. Study area

Mishui basin, a tributary of the Xiangjiang River with a drainage area of 9972 km^2 above the Ganxi hydrologic station, was selected as the study area (Fig. 1). The basin is located southeast of Hunan Province in South China and extends from longitudes 112.85°E to 114.20°E and latitudes 26.00°N to 27.20°N. It has a complex topography, with elevations ranging from 49 m to 2093 m above sea level. The basin's land use is composed of forest and shrubs (54.4%), grassland (33.5%), cropland (11.8%) and urban and water (0.3%). The climate is a humid subtropical monsoon type, with average temperature of approximately 18.0 °C, minimum monthly temperature of approximately 1.5 °C, maximal monthly temperature of approximately 32.0 °C, and mean annual precipitation of approximately 1561 mm, respectively. The temporal and spatial distribution of the precipitation within the Mishui Basin is uneven due to the atmospheric circulation and since most of the annual precipitation occurs between April and September. In these months, particularly in June, basin-wide heavy rains continuously occur, thereby resulting in floods.

3.2. Datasets

The datasets used in the current study include three satellite precipitation products: named TMPA 3B42V6, TMPA 3B42RT, and

Table 1
Parameters commonly calibrated in the Xinanjiang model, their physical meanings, numeric ranges and default values.

Parameter	Physical meaning	Numeric range	Default value	Source
Kc	Ratio of potential evapotranspiration to pan evaporation	0.5–1.5	1	Calibrated
WUM	Water capacity in the upper soil layer (mm)	10–40	20	Calibrated
WLM	Water capacity in the lower soil layer (mm)	50–90	60	Calibrated
WDM	Water capacity in the deeper soil layer (mm)	10–70	60	Calibrated
B	Exponent of the tension water capacity curve	0.1–0.5	0.3	Calibrated
IM	Impervious area accounts for the whole basin area ratio	0–0.1	0.005	LULC data
C	Coefficient of deep evapotranspiration	0.1–0.3	0.2	Calibrated
EX	Exponent of the free water capacity curve	1–1.5	1.2	Calibrated
SM	The free water capacity of the surface soil layer (mm)	10–60	20	Calibrated
KI0	Outflow coefficients of the free water storage to interfolw	0.1–0.5	0.4	KI0 = 0.7-KG0
KG0	Outflow coefficients of the free water storage to groundwater	0.1–0.5	0.3	Calibrated
CI0	Recession constant of the lower interflow storage	0.1–0.9	0.5	Calibrated
CG0	Daily recession constant of groundwater storage	0.9–0.999	0.9	Calibrated
CS0	Recession constant for channel routing	0.1–0.5	0.2	Calibrated
KE	Slot storage coefficient (h)	20–24	24	Calibrated
XE	Flow proportion factor	0.1–0.5	0.5	Calibrated

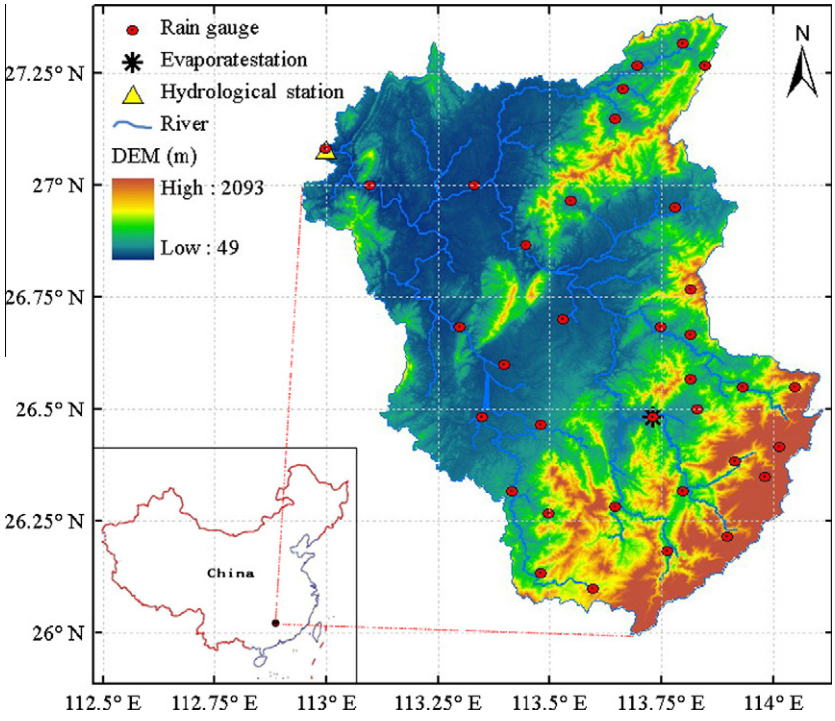

Fig. 1. Map of the Mishui Basin in South China.

CMORPH, ground rain gauge data, potential evaporation data, and streamflow observations at the outlet of the basin.

The 3B42V6 and 3B42RT estimates were provided by TMPA by combining information from multiple satellites at 3 h temporal and 0.25° × 0.25° spatial resolutions, covering the global latitude band from over 50°N to 50°S and 60°N to 60°S respectively. The 3B42RT uses the TRMM Combined Instrument (TCI) dataset, which includes the TRMM precipitation radar (PR) and TRMM Microwave Imager (TMI), to calibrate precipitation estimates derived from available Low Earth Orbit (LEO) microwave (MW) radiometers. The 3B42RT then merges all of the estimates at 3 h intervals; and the gaps in the analyses are filled using Geosynchronous Earth Orbit (GEO) infrared (IR) data regionally calibrated to the merged MW product. The LEO MW data used in TMPA include: Special Sensor Microwave Imager (SSM/I) on Defense Meteorological Satellite Program (DMSP) 13, 14 and 15 satellites, Advanced Microwave Scanning Radiometer-Earth Observing System (AMSR-E) on Aqua, and the National Oceanic and Atmospheric Administration (NOAA)-15, 16, and 17 satellites. The gap-filling IR-based estimates are merged from five GEO satellites (GOES-8 and 10, Meteosat-5 and 7, and GMS-5) into half-hourly 4 km × 4 km equivalent latitude–longitude grids (Janowiak et al., 2001). The 3B42V6 adjusts the monthly accumulations of the 3-h fields from 3B42RT based on a monthly gauge analysis, including the GPCP 1° × 1° monthly rain gauge analysis and the Climate Assessment and Monitoring System (CAMS) 0.5° × 0.5° monthly rain gauge analysis. The 3B42RT is therefore, a near real-time (approximately 3–9 h after real time) product, and 3B42V6 is a post real-time (approximately 10–15 d after the end of each month) research-quality product. The data can be freely downloaded from the following website: http://trmm.gsfc.nasa.gov/.

The CMORPH technique uses the directness of the MW observations with the cloud motion derived from the IR data to estimate precipitation, it is extremely flexible wherein precipitation estimates from any MW satellite source can be incorporated (Joyce et al., 2004). The MW observations used in CMORPH include:

SSM/I on DMSP 13, 14 and 15 satellites, AMSR-E on Aqua, AMSU-B on NOAA-15, 16, and 17 satellites, and TMI on TRMM. The IR data used in CMORPH come from the same satellites with TMPA. Currently, the CMORPH products have two high-resolution versions as follows: one with temporal and spatial resolutions of 3 h and 0.25° respectively, and the other with higher temporal and spatial resolutions of 30 min and 8 km respectively, with both data covering the area from 60°S to 60°N globally. In the present research, the former CMORPH data, being released as an official version, was used. The data can be accessed from the following website: ftp://ftp.cpc.ncep.noaa.gov/precip/global_CMORPH/3-hourly_025deg.

For the two near real-time satellite precipitation products (TMPA 3B42RT and CMORPH), they were estimated form the same data sets except for the TRMM PR used in the TMPA 3B42RT and they both have the same spatial coverage of 60°S to 60°N globally. The main difference between the 3B42RT and CMORPH is just that they adopt different algorithms to retrieve the precipitation.

The observed daily precipitation data from 2003 to 2008 were derived from 35 rain gauge stations in the Mishui basin, roughly two rain gauges within one 0.25° grid, and the same period time series of the daily streamflow and potential evapotranspiration data were collected from the Ganxi hydrologic station and Wulipai evaporation station, respectively. The Inverse Distance Weighting (IDW; Bartier and Keller, 1996) of the three nearest rain gauges was used to obtain the spatial distributed precipitation database of the Mishui basin. The 30 arc-second global digital elevation model data were obtained from the US Geological Survey and the vegetation-type data were obtained from the International Geosphere–Biosphere Program.

The three satellite precipitation products with a 3 h temporal resolution were aggregated to produce the accumulated daily and monthly precipitation for comparison with the interpolated rain gauge data and streamflow simulation. The study period was from 2003 to 2008. Because of this, data from the three satellite precipitation products over 6 years were roundly compared using the evaluation indices and hydrological model described in Section 2 in the Mishui Basin.

4. Results and discussion

4.1. Comparison of satellite precipitation products

To directly compare the three satellite precipitation products with the dense rain gauge observations, the daily basin averaged precipitation time series of the gauge observations and the three satellite precipitation products for the period of 2003–2008 are shown in Fig. 2. The 3B42V6 is shown to have a similar time series with little bias and good CC compared to the gauge observations. The 3B42RT and CMORPH have seriously underestimated the rainfall amount, with biases of −42.72% and −40.81%, respectively. Based on the daily statisticses of areal-based basin gauge and satellite precipitation, as shown in Table 2, 3B42V6 obtained the best values of ME (−0.19 mm), BIAS (−4.54%), POD (0.71), and CSI (0.64), whereas CMORPH obtained the best values of MAE (2.57 mm), CC (0.80), RMSE (6.26 mm) and FAR (0.08). From the daily time series plot and evaluation indices analysis, we can infer that 3B42V6 has a comprehensive better estimation of precipitation than 3B42RT and CMORPH, then CMORPH has a less obvious better estimating than 3B42RT.

To gain further information on the monthly precisions and variations of the three satellite precipitation products, the monthly basin averaged precipitation time series of the gauge observations and the three satellite precipitation products for the same period with the daily series are shown in Fig. 3. Numbers of similar intuitive ideas are shown in comparison with Fig. 2. At the monthly time scale, the 3B42V6 has perfect fitting with the gauge values except the heavy rainfall in August 2007, and the 3B42RT and CMORPH both have significant underestimation of the rainfall. From the monthly statistics of areal-based basin gauge and satellite precipitation products (Table 2), 3B42V6 was observed to obtain all the best values of ME (−5.90 mm), MAE (23.77 mm), BIAS (−4.54), CC (0.94) and RMSE (33.94 mm).

The combinations of the daily and monthly direct analyses comparisons suggest that the 3B42V6 data has considerably improved the monthly precision with a monthly bias adjusted using a global rain gauge analysis data. The monthly bias adjusted method is still imperfect as it could not solve the problems of the daily and sub-daily FAR and missed detection of the rainfall events existed in the 3B42RT and it thus may result in poor detection and estimation of precipitation extent and intensity, particularly during extreme events. The accuracy of the 3B42V6 for the daily and sub-daily time-scale distribution still should provide an increasing possibility to follow the real rainfall situation.

Fig. 4 shows the frequency distribution of daily precipitation in different intensities and their relative contributions to each rainfall event. All the three satellite precipitation products overestimated the occurrence frequency of the no rain event, with frequency of approximately 40%, while the frequency of the gauge observations is only approximately 25%. In terms of 3B42V6, it has an underestimation of the small and moderate rainfall events (0–1, 1–5, 5–10, and 10–20 mm/day) both at occurrence frequency and contribution, while it has an overestimation of the heavy rainfall events (20–30, and $\geqslant$30 mm/day). For 3B42RT and CMORPH, they both underestimated the occurrence frequencies of all the different precipitation intensities; and there are some differences for their contributions compared with the gauge observations: the contribution of $\geqslant$30 mm/day for gauge is 31.38%, while for 3B42RT it is only 17.29%, and for CMORPH it is just 21.53%. In general, the figure shows us that the pure satellite precipitation products (3B42RT and CMORPH) are difficult to reflect the small rainfall events (no rain and 0–1 mm/day) and heavy rainfall events ($\geqslant$30 mm/day) in Mishui basin, and the monthly bias adjusted can improve the frequency and contribution distributions of the near real-time satellite precipitation products.

4.2. Streamflow simulation Scenario I: model calibration with rain gauge data

To evaluate the streamflow prediction utility of the three satellite precipitation products, their effects on streamflow simulations when the model was calibrated based on rain gauge data was first analyzed. The periods of 2003–2005 and 2006–2008 were selected as the calibration and validation periods, respectively. The calibration was processed automatically with the objective function of maximizing the likelihood function, and the model parameters were selected in the experiential numerical range. Fig. 5 shows the daily and monthly comparisons of the observed streamflow with the simulated hydrograph showing the best model parameter estimates for both the calibration and validation periods. Overall, a good agreement exists between the observed and simulated series both in the daily and monthly time scales. The statistical indices, which reflect model performances (with daily CC of 0.95 and 0.92, monthly CC of 0.99 and 0.96, daily NSCE of 0.91 and 0.80, monthly NSCE of 0.97 and 0.91, and BIAS of 1.56% and 5.33% for the calibration period and validation period respectively, see Tables 3 and 4) indicate that the gridded Xinanjiang model captured key features of the observed hydrograph.

Based on the analysis of the calibration and validation simulations from the rain gauge data, the model is believed to be suitably robust in evaluating the utility of the satellite precipitation products for streamflow simulation. The calibrated gridded Xinanjiang

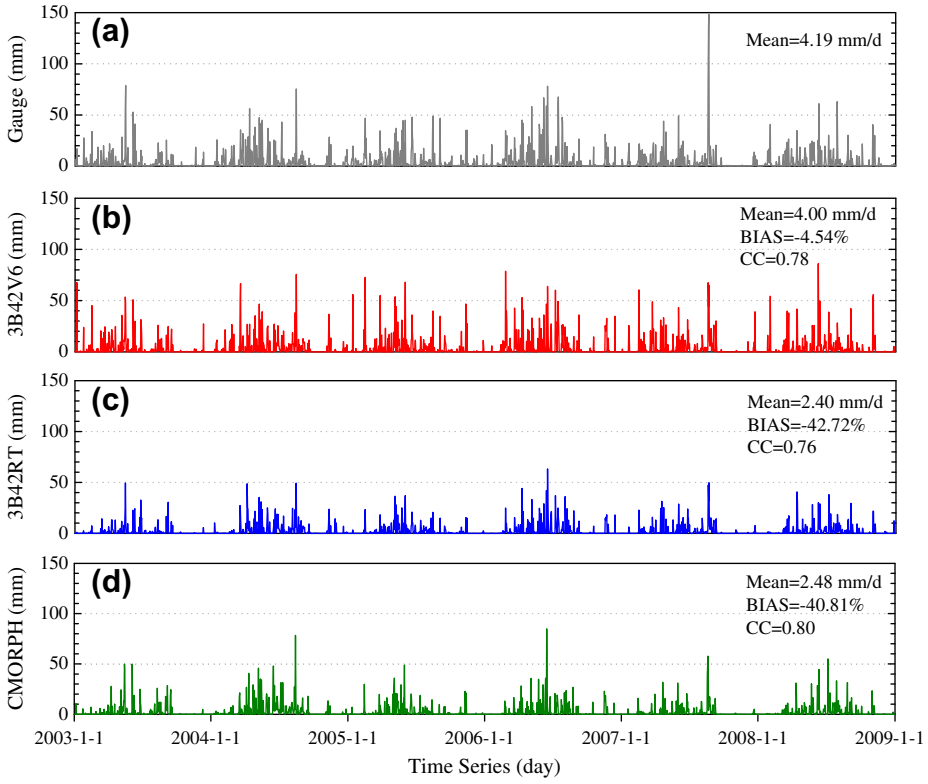

Fig. 2. Daily basin averaged precipitation time series of the gauge observations and the three satellite precipitation products for the period of 2003–2008.

Table 2
Statisticses of areal-based basin gauge observations and satellite precipitation products both at daily and monthly time scales.

Precipitation products	Mean	ME	MAE	BIAS	CC	RMSE	POD	FAR	CSI
Daily time series									
Gauge	4.19	–	–	–	–	–	–	–	–
3B42V6	4.00	−0.19	2.63	−4.54	0.78	6.42	0.71	0.13	0.64
3B42RT	2.40	−1.79	2.81	−42.72	0.76	6.80	0.58	0.13	0.54
CMORPH	2.48	−1.71	2.57	−40.81	0.80	6.26	0.61	0.08	0.58
Monthly time series									
Gauge	127.57	–	–	–	–	–	–	–	–
3B42V6	121.66	−5.90	23.77	−4.54	0.94	33.94	–	–	
3B42RT	72.96	−54.61	56.85	−42.72	0.88	72.63	–	–	–
CMORPH	75.65	−51.91	57.73	−40.81	0.85	72.78	–	–	–

Table 3
Daily statistical measures of precipitation inputs and corresponding streamflows for the calibration and validation periods.[a]

Precipitation products	Precipitation input		Simulated streamflow (Scenario I)			Simulated streamflow (Scenario II)		
	CC	BIAS (%)	CC	NSCE	BIAS (%)	CC	NSCE	BIAS (%)
Calibration period								
Gauge	–	–	0.95	0.91	1.56	–	–	–
3B42V6	0.81	−2.92	0.77	0.55	−3.52	0.77	0.57	−4.42
3B42RT	0.73	−42.95	0.67	0.11	−58.58	0.71	0.46	−4.66
CMORPH	0.81	−34.72	0.65	0.25	−48.34	0.70	0.43	4.18
BMA_2	–	–	–	–	–	0.73	0.50	−0.23
BMA_3	–	–	–	–	–	0.77	0.58	−1.67
Validation period								
Gauge	–	–	0.92	0.80	5.33	–	–	–
3B42V6	0.77	−6.13	0.75	0.56	−4.18	0.76	0.57	0.59
3B42RT	0.78	−42.68	0.72	0.21	−65.39	0.79	0.57	−25.47
CMORPH	0.82	−45.93	0.69	0.18	−70.67	0.81	0.58	−17.60
BMA_2	–	–	–	–	–	0.81	0.60	−22.02
BMA_3	–	–	–	–	–	0.83	0.62	−14.22

[a] *Notation*: In Scenario I, the model parameters is calibrated based on the rain gauge data, we calculated the statistical measures in calibration and validation periods respectively just for corresponding comparison with Scenario II.

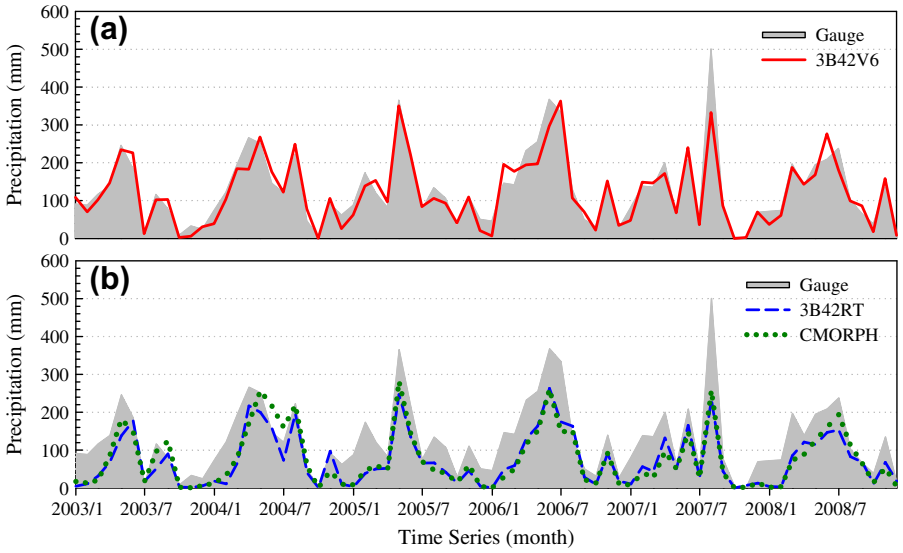

Fig. 3. Monthly basin averaged precipitation time series of the gauge observations and the three satellite precipitation products for the period of 2003–2008.

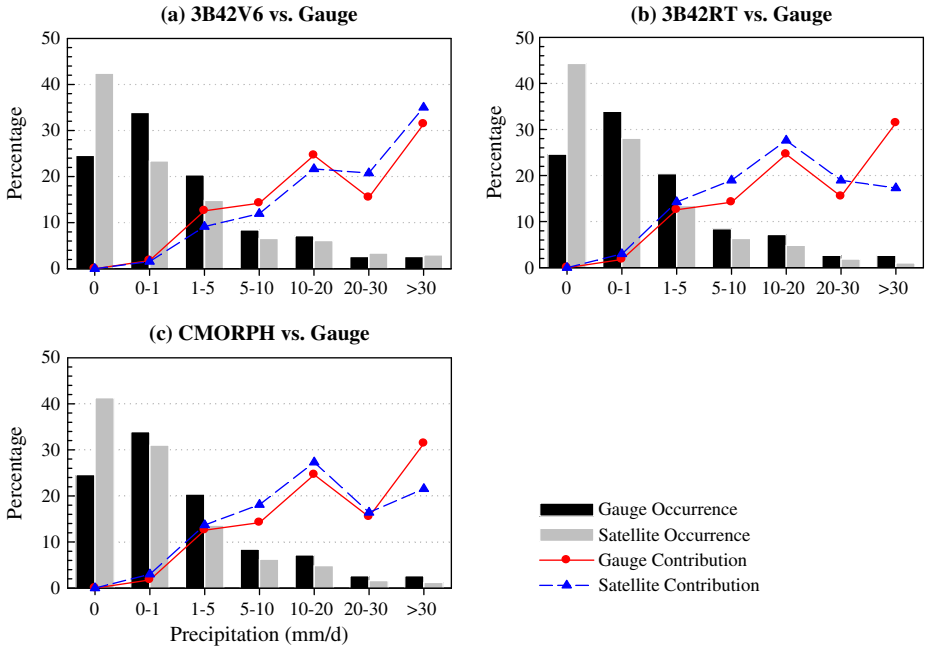

Fig. 4. Occurrence frequencies of different precipitation products and their relative contributions to the total rainfall.

model was then forced by the three satellite precipitation products as inputs during the period from 2003 to 2008. The simulation from the 3B42V6 data, which had daily CC of 0.77 and 0.75, monthly CC of 0.94 and 0.89, daily NSCE of 0.55 and 0.56, monthly NSCE of 0.88 and 0.80, and BIAS of −3.52% and −4.18% for the calibration and validation periods, respectively, was shown to fit best with the observed streamflow series amongst the three products (see Fig. 6, Tables 3 and 4). Still, the simulation underestimated some high peak flows in the rainy seasons and overestimated some low peak flows in the dry seasons that were attributable to the 3B42V6 data uncertainty at the daily time scale (Fig. 2).

The simulations of the 3B42RT and CMORPH data significantly underestimated most of the streamflow series because of their systematic underestimation of precipitation. The simulation from the 3B42RT had daily CC of 0.67 and 0.72, daily NSCE of 0.11 and 0.21 and BIAS of −58.58% and −65.39% for the calibration and validation periods, respectively. The simulation from the CMORPH had daily CC of 0.65 and 0.69, daily NSCE of 0.25 and 0.18, and BIAS of −48.34% and −70.67% for the calibration and validation periods, respectively (Table 3).

4.3. Streamflow simulation Scenario II: model calibration with each satellite data

The streamflow simulation utility of the three satellite precipitation products were assessed further by calibrating the model with the corresponding satellite precipitation data. The calibration and validation periods were same to that of Scenario I. Fig. 7 shows the comparisons of the observed and simulated streamflows. Combining the daily and monthly statistical analyses shown in Tables 3 and 4, the performances of the simulation from the two near real-time satellite products have obviously improved after the

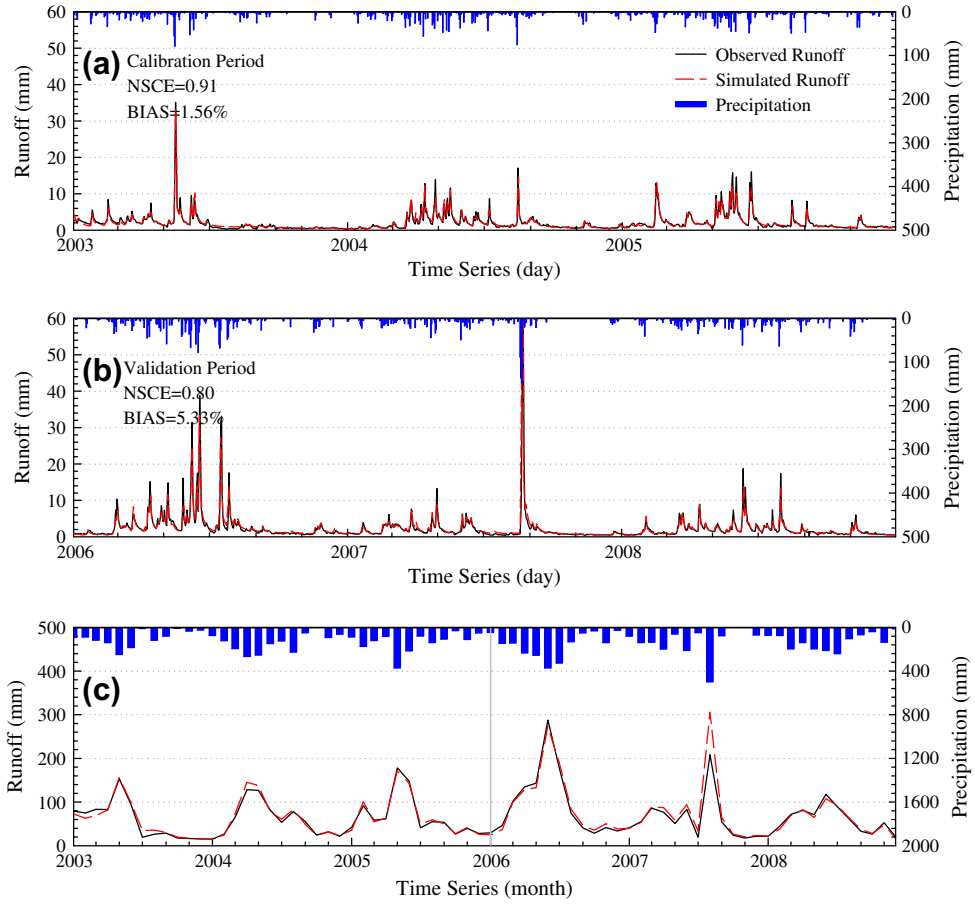

Fig. 5. Observed and simulated streamflows using rain gauge data as input: (a) daily calibration period, (b) daily validation period, and (c) monthly time series.

Table 4
Monthly statistical measures of precipitation inputs and corresponding streamflows for the calibration and validation periods.

Precipitation products	Precipitation input		Simulated streamflow (Scenario I)			Simulated streamflow (Scenario II)		
	CC	BIAS (%)	CC	NSCE	BIAS (%)	CC	NSCE	BIAS (%)
Calibration period								
Gauge	–	–	0.99	0.97	1.56	–	–	–
3B42V6	0.95	−2.92	0.94	0.88	−3.52	0.92	0.84	−4.42
3B42RT	0.87	−42.95	0.78	−0.23	−58.58	0.83	0.66	−4.66
CMORPH	0.84	−34.72	0.68	−0.04	−48.34	0.76	0.53	4.18
BMA_2	–	–	–	–	–	0.81	0.63	−0.23
BMA_3	–	–	–	–	–	0.87	0.75	−1.67
Validation period								
Gauge	–	–	0.96	0.91	5.33	–	–	–
3B42V6	0.93	−6.13	0.89	0.80	−4.18	0.89	0.80	0.59
3B42RT	0.90	−42.68	0.87	−0.11	−65.39	0.93	0.75	−25.47
CMORPH	0.89	−45.93	0.84	−0.25	−70.67	0.89	0.67	−17.60
BMA_2	–	–	–	–	–	0.92	0.73	−22.02
BMA_3	–	–	–	–	–	0.95	0.82	−14.22

parameters were recalibrated, whereas the simulation from the 3B42V6 data had minor changes. The simulation from the 3B42RT data had daily CC of 0.71 and 0.79, monthly CC of 0.83 and 0.93, daily NSCE of 0.46 and 0.57, monthly NSCE of 0.66 and 0.75, and BIAS of −4.66% and −25.47% for the calibration and validation periods, respectively. The simulation from the CMORPH data had daily CC of 0.70 and 0.81, monthly CC of 0.76 and 0.89, daily NSCE of 0.43 and 0.58, monthly NSCE of 0.53 and 0.67, and BIAS of 4.18% and −18.59% for the calibration and validation periods, respectively. The streamflow simulations from the 3B42RT and CMORPH showed comparable results with the simulation from the 3B42V6 except their bigger biases in validation period.

4.4. Merging the simulations using BMA

The streamflow simulations from different satellite precipitation datasets have their respective advantages. At the daily time scale, the 3B42V6 has the best CC (0.77) and NSCE (0.57), and the CMORPH has the best BIAS (4.18%) in the calibration period; and the CMORPH has the best CC (0.81) and NSCE (0.58), and the 3B42V6 has the best BIAS (0.59%) in the validation period. Merging different kinds of simulations may generate a better and more stable streamflow series. In the current study, the feasibility of merging different streamflow series simulated from the three satellite precipitation products was evaluated. Two different merging cases

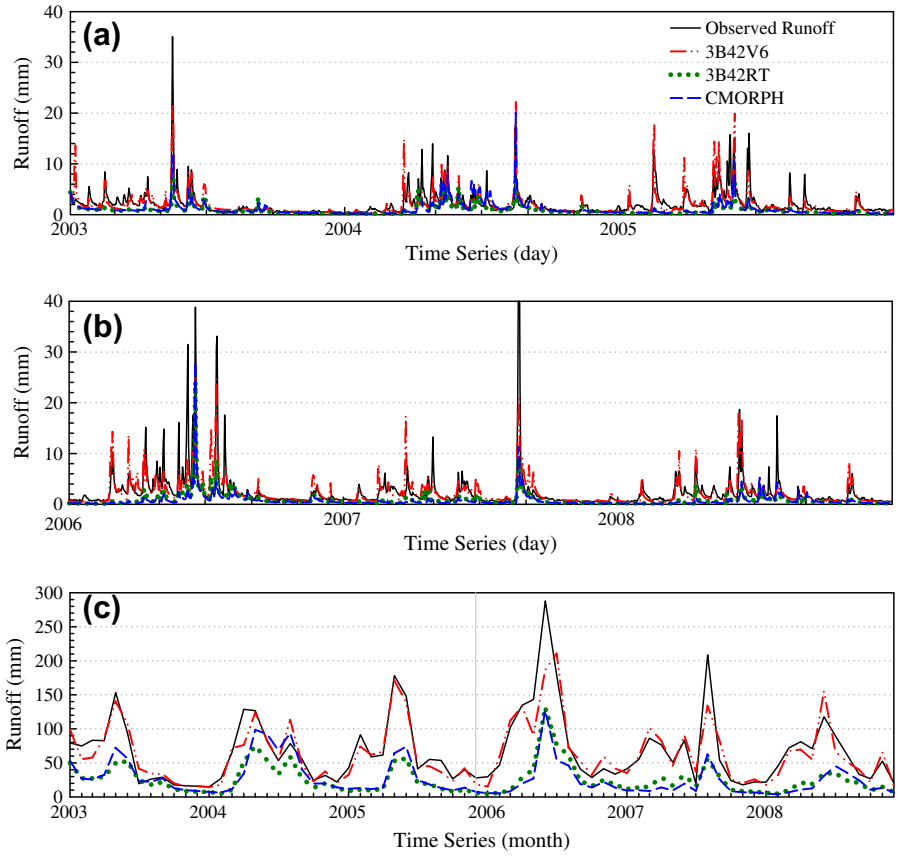

Fig. 6. Observed and simulated streamflows from the three satellite precipitation products with gauge calibrated parameters: (a) daily calibration period, (b) daily validation period, and (c) monthly time series.

were conducted. In case one, we merged the streamflow simulations from the two near real-time satellite precipitation products (3B42RT and CMORPH) via the BMA method (which is named *BMA_2*). This merging method will be useful for the future practical near real-time streamflow forecasting. In case two, we merged the streamflow simulations from the three satellite precipitation products using the BMA method (which is named *BMA_3*). This merging method will be useful for the future water balance analysis, and water resources planning and management.

Fig. 8 shows the comparison of the observed and merged streamflow series using the BMA method, while Tables 3 and 4 show the calculated daily and monthly statistical indices. These findings show that: the new merged streamflow series of *BMA_2* has better daily CC (0.73 and 0.81), higher daily NSCE (0.50 and 0.60) and comparable BIAS (−0.23% and −22.02%) compared with each individual satellite simulation from the two near real-time satellite precipitation products during both the calibration and validation periods; and the new merged streamflow series of *BMA_3* has better daily CC (0.78 and 0.83), higher daily NSCE (0.58 and 0.62) and comparable BIAS (−1.67% and −14.22%) compared with each individual satellite simulation from the three satellite precipitation products for the calibration and validation periods respectively. For the monthly time series, the merged results are similar to the best of the simulations from the single satellite precipitation product. The results show that the BMA merging method effectively improved the daily streamflow series to a better and more stable direction in terms of both CC and NSCE, though suffered from the high biases of the 3B42RT and CMORPH in validation period. For the merged streamflow series, some high flows for the flood seasons were still underestimated due to the inherited relatively low spatial resolution of current TRMM-era satellite precipitation products.

4.5. Comprehensive analysis of the two simulation scenarios and the merging results

The statistical indices of daily NSCE and BIAS for the validation period from Table 3 were selected for the visual comparison of the satellite streamflow simulations performance based on the two simulation scenarios and BMA merged results, as shown in Fig. 9. Comparing the simulations of the 3B42V6 with those of the 3B42RT and CMORPH based on rain gauge calibrated parameters, the smaller rainfall bias of the 3B42V6 was found to be tolerated by the error propagation and integration of the Xinanjiang modelling processes, whereas the bias of the streamflow simulation from the 3B42R and CMORPH were larger than that of the 3B42V6. The model recalibration had significantly improved the NSCE values and reduced the BIAS values of the two near real-time satellite precipitation data sets compared with the performances based on the rain gauge parameters. By contrast, the BMA merging method resulted in better NSCE values (0.50 and 0.60) for the syncretic streamflow series of *BMA_2* compared with the former single better values of 3B42RT (0.46) and CMORPH (0.58) for the calibration period and validation period respectively; and better NSCE values (0.58 and 0.62) for the syncretic streamflow series of *BMA_3* compared with the former single best values of 3B42V6 (0.57) and CMORPH (0.58) for the calibration period and validation period respectively. It was noted, however, that the merging of *BMA_3* also resulted in a moderately decreased bias value from the single best 3B42V6 during the validation period, likely due to the contamination of two real-time satellite products. In the present work, the merging approach demonstrated a positive transformation of NSCE and BIAS. It was noted though that the merging approach still suffered from the high variability of the two near real-time satellite precipitation products.

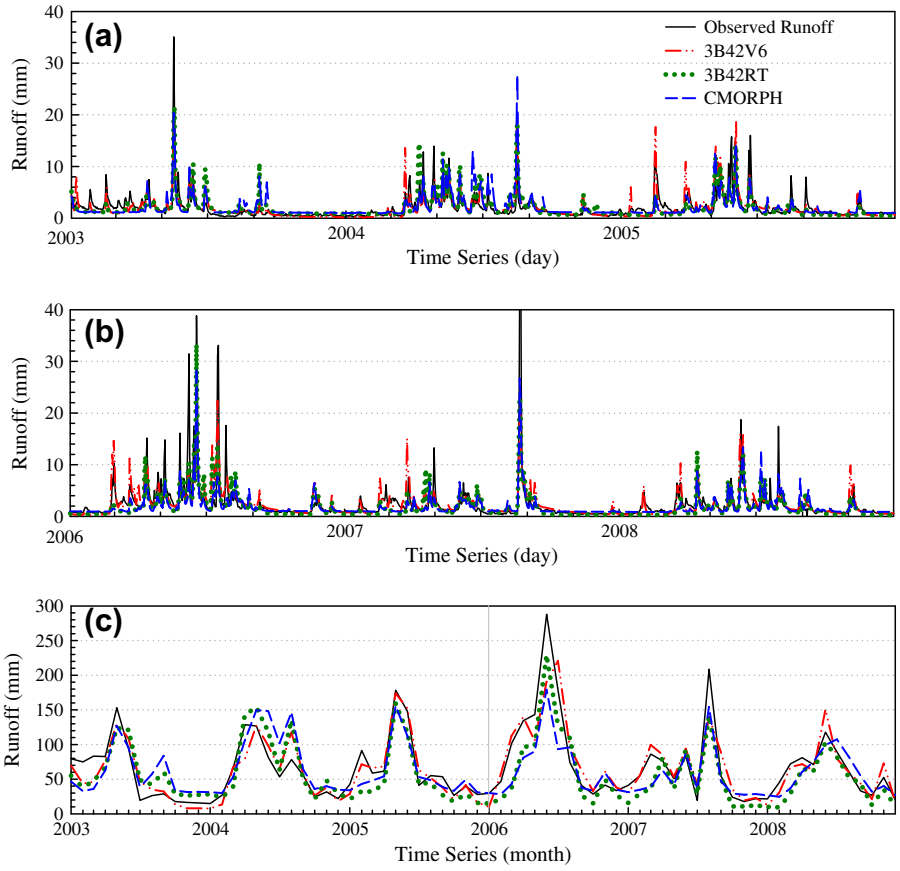

Fig. 7. Observed and simulated streamflows from the three satellite precipitation products with recalibrated parameters: (a) daily calibration period, (b) daily validation period, and (c) monthly time series.

Table 5 shows the parameters of the gridded Xinanjiang model calibrated with each specific precipitation data as input for the calibration period of 2003–2005, which are the mean values of the 10,000 groups of the calibrated parameters when the SCEM-UA algorithm was converged. The variations of the model parameters with respect to each different precipitation input were further analysed. Five parameters, including Kc, WUM, WLM, WDM, and *C* were used in the evapotranspiration calculation. Kc is a ratio of potential evapotranspiration to pan evaporation. When the Kc value is increased, the calculated evapotranspiration also increases; conversely, the evapotranspiration decreases. For the much larger negative bias (underestimation) of the 3B42RT and CMORPH, the recalibration reduced the Kc values for a good simulation of the streamflow. WUM, WLM, and WDM refer to the water capacities of the three soil layers, and *C* is the conversion coefficient of deep evapotranspiration. These parameters have similar changes compared with that of the Kc. The other parameters did not have obvious and regular changes. Because of this, the parameter recalibration of each satellite precipitation product as well as the improved performance of the streamflow simulation came at the expense of decreasing the performance of the evapotranspiration calculation by adjusting the sensitive model parameters that affect the water balance. Bitew and Gebremichael (2011) also emphasized that this trade-off is an inevitable consequence of the error in satellite precipitation estimates and the focus of the calibration strategy.

4.6. Comparing with the findings of some other studies

In recent years, there have been many research attempts at conducting an evaluation regarding the accuracy and the hydrological prediction utility of the multi-satellite precipitation products. Many of them draw similar conclusions as this study: the near real-time pure satellite precipitation products exist varying bias in different basins. The monthly bias adjusted research-quality TMPA 3B42V6 data has much better precision compared to the pure satellite precipitation products. When using the pure satellite precipitation products with large bias to do streamflow simulation, the parameter recalibrated based on corresponding satellite data can improve the simulation performance of the streamflow. Yong et al. (2010) pointed out that the biases of the 3B42V6 and 3B42RT in the Laohahe basin (with area of 18,112 km^2, longitudes 94.5°W to 94.06°W and latitudes 35.85°N to 36.37°N) are 16.52% and 76.94% respectively, the VIC-3L model can tolerate the non-physical overestimation of the 3B42V6 and the 3B42RT has weak hydrologic utility. Behrangi et al. (2011) found that the biases of the 3B42V6, 3B42RT and CMORPH in the Illinois River basin (with area of 1489 km^2, longitudes 94.5°W to 94.06°W and latitudes 35.85°N to 36.37°N) are 1.7%, 34.5% and 40.1% respectively, and the bias-adjustment and parameters recalibration are critical steps in improving the applicability of the near real-time satellite precipitation products for streamflow simulation. Still, there are some different findings with respect of the satellite-based precipitation accuracy. For example, Bitew and Gebremichael (2011) discovered that the biases of the 3B42V6, 3B42RT and CMORPH in a mountain Gilgel Abay basin (with area of 1656 km^2, longitudes 36.8°W to 37.4°W and latitudes 10.93°N to 11.38°N) are −64%, −29% and −29% respectively. The 3B42V6 shows inconsistencies and the lowest performance of the streamflow simulation. This may be due to the low density of rain gauges in a complex terrain region used for bias adjusted and the incapability of the merging algorithm to factor this.

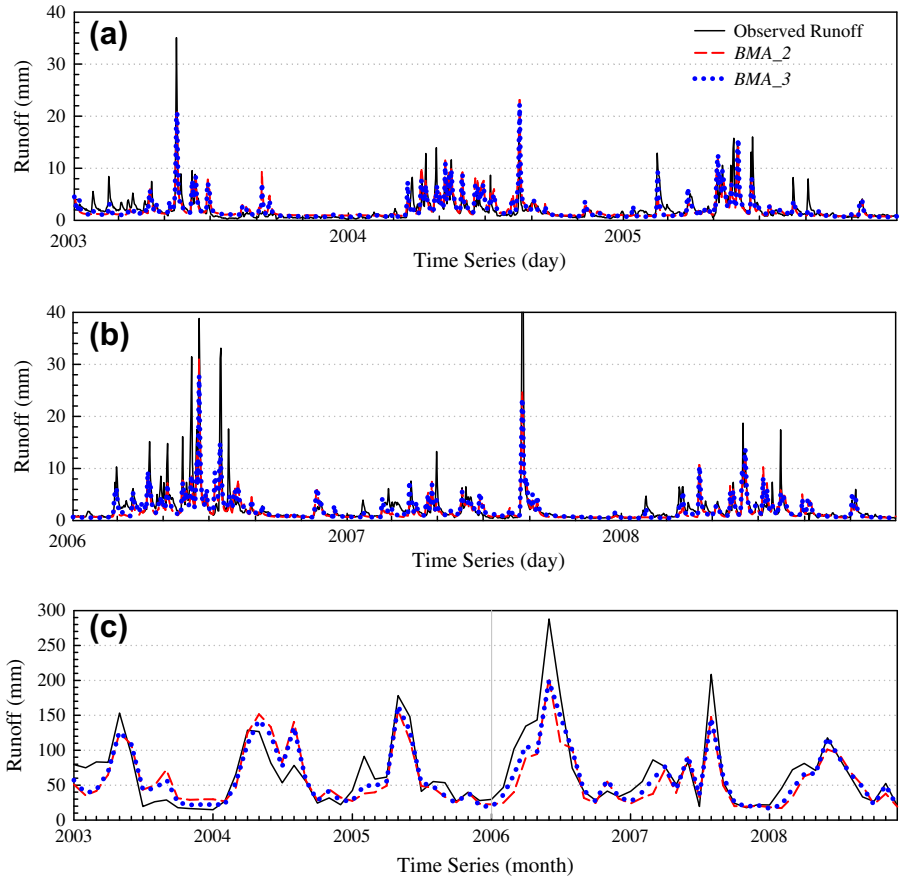

Fig. 8. Observed and two merged streamflows using BMA method: (a) daily calibration period, (b) daily validation period, and (c) monthly time series.

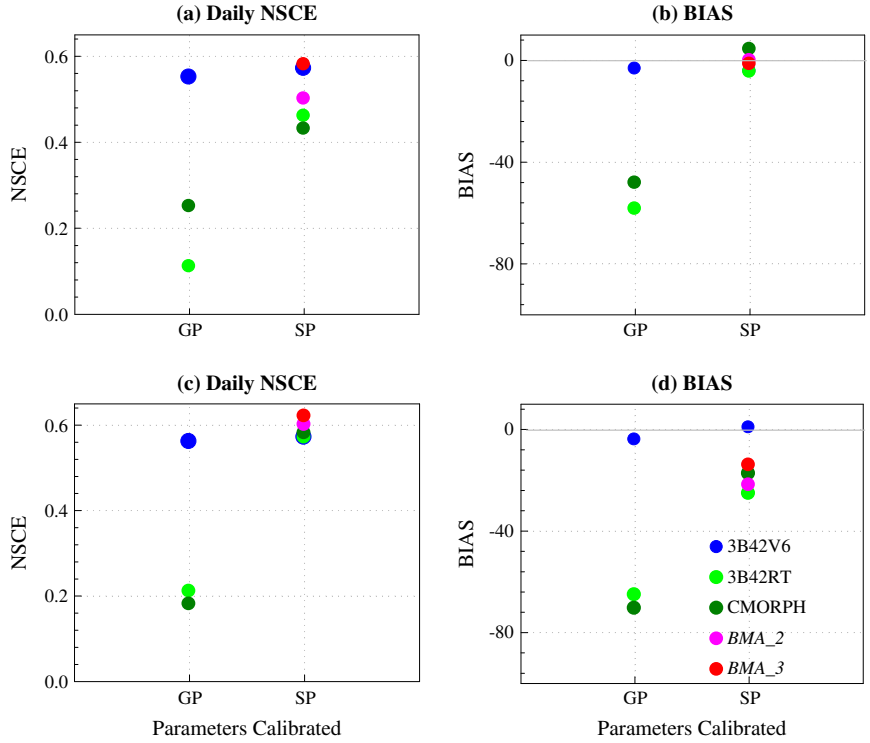

Fig. 9. Comparison of the performance statisticses of the three satellite streamflow simulations for the two simulation scenarios and BMA merged results: (a) NSCE for the calibration period, (b) BIAS for the calibration period, (c) NSCE for the validation period, and (d) BIAS for the validation period.

Table 5
Gridded Xinanjiang model parameter values obtained from the calibrated model with different precipitation data as inputs for the calibration period of 2003–2005.[a]

Parameters	Gauge	3B42V6	3B42RT	CMORPH
Kc	1.39	1.40	0.76	0.73
WUM	36.08	38.83	19.48	15.20
WLM	82.67	78.53	74.21	75.92
WDM	24.43	25.56	18.82	19.49
B	0.49	0.39	0.47	0.31
C	0.27	0.15	0.19	0.13
Ex	1.30	1.25	1.10	1.30
SM	27.23	33.79	12.75	26.76
KG0	0.35	0.44	0.14	0.36
CI0	0.81	0.54	0.70	0.57
CG0	0.99	0.99	0.99	0.99
CS0	0.11	0.25	0.23	0.19
KE	20.36	20.28	20.39	20.41
XE	0.49	0.49	0.49	0.49

[a] The parameter values are the mean values of the 10,000 groups of calibrated parameters when the SCEM-UA algorithm was convergent.

5. Conclusions

Satellite precipitation products provide new kinds of input data (i.e. uninterrupted and global coverage) for various hydrologic models which are very important for regional and global hydrologic prediction and water resources management worldwide. This is especially useful for data-spare and ungauged basins. In the current study, the accuracy and the streamflow simulation utility of three most widely used high-resolution satellite precipitation products (TMPA 3B42V6, TMPA 3B42RT and CMORPH) which were evaluated within the Mishui Basin, South China, and their simulations were merged using the Bayesian model averaging method. The analyses support the following conclusions:

In the Mishui basin, larger underestimation biases were observed for the two near real-time satellite precipitation products, and the 3B42V6, with a low bias of −4.54%, fitted best with the rain gauge observations at a monthly scale, though with some modest inconsistence at the daily time scale. When the gridded Xinanjiang model was benchmarked by the rain gauge data, the performance of streamflow simulations from the three satellite precipitation products were compatible and obviously effected by their precipitation forcing data quality.

Based on the error propagation and integration of the hydrological modeling processes, the 3B42V6 had not just the best simulation of the streamflow but also the forcing data uncertainty was tolerated. This effectively reduced the error in streamflow simulations, whereas the 3B42RT and CMORPH, due to their higher forcing data uncertainty beyond the hydrological model's tolerance threshold, resulted in amplified error propagation into the streamflow simulation. After recalibrating the parameters for each specific satellite precipitation product, the significant negative biases (i.e. underestimation) of both the 3B42RT and the CMORPH data were effectively taken into account by the recalibrated parameters for the streamflow simulation. These improved simulations of streamflow, however, as a major compromise, notably worsened the performance of the evapotranspiration calculation.

The optimal merging of the individual satellite streamflow simulations using the BMA method achieved the best CC and NSCE values of the streamflow series at the daily time scale for both the calibration and validation periods. Still, the merging also resulted in a moderately decreased bias value from the single best 3B42V6 result, particularly during the validation period. This was likely caused from the high variability of the two near real-time satellite precipitation products. Overall, the merging approach demonstrated a positive transformation of the NSCE and BIAS, effectively averaging the bias. We plan to further investigate this BMA merging approach in other basins, where the accuracies of the three satellite precipitation products are similar; also we can introduce more satellite precipitation products.

In summary, the three current state-of-the-art satellite precipitation products have significant potential in hydrological research and applications. The benchmarking, recalibration, and optimal merging schemes using multi-satellite precipitation products for streamflow simulation described in the present work will hopefully be a good reference for future utilizations of various satellite precipitation products in global and regional hydrological applications. This would especially be the case for the data-sparse and ungauged basins.

Acknowledgments

The current study was supported by the Programme of Introducing Talents of Discipline to Universities by the Ministry of Education and the State Administration of Foreign Experts Affairs, China (the 111 Project, No. B08048), the Innovative Research Team Project of the State Key Laboratory of Hydrology-Water Resources and Hydraulic Engineering (No. 2009585412), and the National Science Foundation for Young Scientists of China (No. 40901017). The present work was also funded by the Special Basic Research Fund by the Ministry of Science and Technology, China (No. 2011IM011000) and the Fundamental Research Funds for the Central Universities (No. 2011B01814). We also acknowledge the HyDROS Lab (HyDRometeorology and RemOte Sensing Laboratory: http://hydro.ou.edu) at the National Weather Center, Norman, OK for their guidance and support.

References

Ajami, N.K., Duan, Q.Y., Sorooshian, S., 2007. An integrated hydrological Bayesian multimodel combination framework: confronting input, parameter, and model structural uncertainty in hydrologic prediction. Water Resour. Res. 43, W01403.
Bartier, P.M., Keller, C.P., 1996. Multivariate interpolation to incorporate thematic surface data using inverse distance weighting (IDW). Comput. Geosci. 22, 795–799.
Behrangi, A., Khakbaz, B., Jaw, T.C., AghaKouchak, A., Hus, K., Sorooshian, S., 2011. Hydrologic evaluation of satellite precipitation products over a mid-size basin. J. Hydrol. 397, 225–237.
Bitew, M.M., Gebremichael, M., 2011. Evaluation of satellite rainfall products through hydrologic simulation in a full distributed hydrologic model. Water Resour. Res. 47, W06526.
Chiang, Y.M., Hsu, K.L., Chang, F.J., Hong, Y., Sorooshian, S., 2007. Merging multiple precipitation sources for flash flood forecasting. J. Hydrol. 340, 183–196.
Chokngamwong, R., Chiu, L.S., 2008. Thailand daily rainfall and comparison with TRMM products. J. Hydrometeorol. 9, 256–266.
Duan, Q.Y., Sorooshian, S., Gupta, V.K., 1994. Optimal use of the SCE-UA global optimization method for calibrating watershed models. J. Hydrol. 158, 265–284.
Duan, Q.Y., Ajami, N.K., Gao, X.G., Sorooshian, S., 2007. Multi-model ensemble hydrologic prediction using Bayesian model averaging. Adv. Water Resour. 30, 1371–1386.
Dinku, T., Chidzambwa, S., Ceccato, P., Connor, S.J., Ropelewski, C.F., 2008. Validation of high-resolution satellite rainfall products over complex terrain. Int. J. Remote Sens. 29, 4097–4110.
Ebert, E.E., Janowiak, J.E., Kidd, C., 2007. Comparison of near-real-time precipitation estimates from satellite observations and numerical models. Bull. Am. Meteorol. Soc. 88, 47–64.
Gebregiorgis, A., Hossain, F., 2011. How much can a priori hydrologic model predictability help in optimal merging of satellite precipitation products. J. Hydrometeorol. 12, 1287–1298.
Hong, Y., Hsu, K.L., Sorooshian, S., Gao, X.G., 2004. Precipitation estimation from remotely sensed imagery using artificial neural network-cloud classification system. J. Appl. Meteorol. 43, 1834–1852.
Hong, Y., Adler, R.F., Hossain, F., Curtis, S., Huffman, G.J., 2007. A first approach to global runoff simulation using satellite rainfall estimation. Water Resour. Res. 43, W08502.
Huffman, G.J., Adler, R.F., Bolvin, D.T., Gu, G.J., Nelkin, E.J., Bowman, K.P., Hong, Y., Stocker, E.F., Wolff, D.B., 2007. The TRMM multi-satellite precipitation analysis (TMPA): quasi-global, multi-year, combined-sensor precipitation estimates at fine scales. J. Hydrometeorol. 8, 38–55.
Janowiak, J.E., Joyce, R.J., Yarosh, Y., 2001. A real-time global half-hourly pixel-resolution infrared dataset and its applications. Bull. Am. Meteorol. Soc. 82, 205–217.

Joyce, R.J., Janowiak, J.E., Arkin, P.A., Xie, P.P., 2004. CMORPH: a method that produces global precipitation estimates from passive microwave and infrared data at high spatial and temporal resolution. J. Hydrometeorol. 5, 487–503.

Jiang, S.H., Ren, L.L., Yong, B., Yang, X.L., Shi, L., 2010. Evaluation of high-resolution satellite precipitation products with surface rain gauge observations from Laohahe basin in northern China. Water Sci. Eng. 3, 405–417.

Kubota, T., Shige, S., Hashizume, H., Aonashi, K., Takahashi, N., Seto, S., Hirose, M., Takayabu, Y.N., Ushio, T., Nakagawa, K., Iwanami, K., Kachi, M., Okamoto, K., 2007. Global precipitation map using satellite borne microwave radiometers by the GSMaP project: production and validation. IEEE Trans. Geosci. Remote Sens. 45, 2259–2275.

Liang, X., Lettenmaier, D.P., Wood, E.F., Burges, S.J., 1994. A simple hydrologically based model of land surface water and energy fluxes for GSMs. J. Geophys. Res. 99, 14415–14428.

Liang, X., Wood, E.F., Lettenmaier, D.P., 1996. Surface soil moisture parameterization of the VIC-2L model: evaluation and modification. Global Planet. Change 13, 195–206.

Li, M., Shao, Q.X., 2010. An improved statistical approach to merge satellite rainfall estimates and raingauge data. J. Hydrol. 385, 51–64.

Nash, J.E., Sutcliffe, J.V., 1970. River flow forecasting through conceptual models. Part 1: a discussion of principles. J. Hydrol. 10, 282–290.

Sorooshian, S., Hsu, K.L., Gao, X.G., Gupta, H.V., Imam, B., Braithwaite, D., 2000. Evaluation of PERSIANN system satellite-based estimates of tropical rainfall. Bull. Am. Meteorol. Soc. 81, 2035–2046.

Su, F., Hong, Y., Lettenmaier, D.P., 2008. Evaluation of TRMM multi-satellite precipitation analysis (TMPA) and its utility in hydrologic prediction in La Plata basin. J. Hydrometeorol. 9, 622–640.

Stisen, S., Sandholt, I., 2010. Evaluation of remote-sensing-based rainfall products through predictive capability in hydrological runoff modeling. Hydrol. Process. 7, 879–891.

Turk, F.J., Miller, S.D., 2005. Toward improved characterization of remotely sensed precipitation regimes with MODIS/AMSR-E blended data techniques. IEEE Trans. Geosci. Remote Sens. 43, 1059–1069.

Tian, Y.D., Peters-Lidard, C.D., Choudhury, B.J., Garcia, M., 2007. Multitemporal analysis of TRMM-based satellite precipitation products for land data assimilation applications. J. Hydrometeorol. 8, 1165–1183.

Turk, F.J., Arkin, P., Ebert, E.E., Sapiano, M.R.P., 2008. Evaluation high-resolution precipitation products. Bull. Am. Meteorol. Soc. 87, 1911–1916.

Vrugt, J.A., Gupta, H.V., Bouten, W., Sorooshian, S., 2003. A shuffled complex evolution metropolis algorithm for optimization and uncertainty assessment of hydrologic model parameters. Water Resour. Res. 39, 1201.

Yu, Z.F., Yu, H., Chen, P.Y., Qian, C.H., Yue, C.J., 2009. Verification of tropical cyclone-related satellite precipitation estimates in mainland China. J. Appl. Meteorol. Climatol. 48, 2227–2241.

Yong, B., Ren, L.L., Hong, Y., Wang, J.H., Gourley, J.J., Jiang, S.H., Chen, X., Wang, W., 2010. Hydrologic evaluation of multisatellite precipitation analysis standard precipitation products in basins beyond its inclined latitude band: a case study in Laohahe basin, China. Water Resour. Res. 46, W07542.

Yong, B., Hong, Y., Ren, L.L., Gourley, J.J., Huffman, G.J., Chen, X., Wang, W., Khan, S., 2012. Assessment of evolving TRMM-based multi-satellite real-time precipitation estimation methods and their impacts on hydrologic prediction in a high latitude basin. J. Geophys. Res. – Atmos. 117, D09108.

Yilmaz, M.T., Houser, P., Sherestha, R., Anantharaj, V.G., 2010. Optimally merging precipitation to minimize land surface modeling errors. J. Appl. Meteorol. Climatol. 49, 415–423.

Zhao, R.J., 1992. The Xinanjiang model applied in China. J. Hydrol. 135, 371–381.